JOURNAL OF GEOPHYSICAL RESEARCH, VOL. 104, NO. A5, PAGES 10,295–10,306, MAY 1, 1999

# Nonlinear kinetic modeling of early stage plasmaspheric refilling

M. W. Liemohn[1], G. V. Khazanov[2], P. D. Craven[3], and J. U. Kozyra[1]

**Abstract.** A new time-dependent kinetic model is used to investigate the effects of self-consistency and hot plasma influences on plasmaspheric refilling. The model employs a direct solution of the kinetic equation with a Fokker-Planck Coulomb collision operator to obtain the phase space distribution function of the thermal protons along a field line. Of particular interest is the influence of several processes on the source cone distribution function formation. It is found that a self-consistent ion temperature in the collision term can increase or decrease the equatorial plane density, depending not only on the choice of ion temperature in the static-background calculations but also on the form of the nonlinear representation. The inclusion of a self-consistent polarization electric field increases the early stage equatorial plane density by a factor of 2. Investigations of the effects of anisotropic hot plasma populations on the refilling rates shows that, after a slight initial decrease in equatorial density from clearing out the initial distribution, there is a 10 to 30% increase after 4 hours due to these populations. This increase is due primarily to a slowing of the refilling streams near the equator from the reversed electric field.

## 1. Introduction

Numerous measurements of plasmaspheric refilling of the cold ions have been reported over the years [e.g., *Park*, 1970; *Sojka et al.*, 1983; *Wrenn et al.*, 1984; *Chandler and Chappell*, 1986; *Song et al.*, 1988; *Carpenter and Anderson*, 1992; *Elphic et al.*, 1996; *Lawrence et al.*, 1999]. Modeling studies of this process have also been conducted for several decades now using a variety of numerical techniques, such as hydrodynamic approaches [*Banks et al.*, 1971; *Schulz and Koons*, 1972; *Khazanov et al.*, 1984; *Singh et al.*, 1986; *Rasmussen and Schunk*, 1988; *Guiter and Gombosi*, 1990], semi-kinetic particle-in-cell techniques [*Singh*, 1988; *Wilson et al.*, 1992; *Miller et al.*, 1993], and more global hydrodynamic approaches [*Rasmussen et al.*, 1993; *Weiss et al.*, 1997; *Ober et al.*, 1997]. Another class of plasmasphere models is based on an exospheric approach [*Pierrard and Lemaire*, 1996; *Reynolds et al.*, 1997], but these are steady state models and are not applicable for modeling the refilling process. There have also been several reviews of this topic [e.g., *Horwitz*, 1987; *Singh and Horwitz*, 1992; *Singh et al.*, 1994].

Various timescales and populations have been identified as part of the refilling process. Intervals range from the supersonic interhemispherical flows that last less than an hour [e.g., *Singh*, 1991; *Guiter et al.*, 1995] to the slow subsonic refilling that can last several days [e.g., *Miller et al.*, 1993]. The populations include an isotropic cold plasma of less than a few eV, field-aligned beams of cold plasma, and warm anisotropic particles with a perpendicular temperature up to 20 eV [see *Sojka et al.*, 1983]. The counterstreaming beams are clearly the refilling source from the ionospheric footpoints, and the isotropic population is the preexisting or newly refilled thermal population, while the anisotropic distributions have been attributed to ion cyclotron heating in the equatorial region [*Horwitz et al.*, 1981; *Curtis*, 1985; *Olsen et al.*, 1987, 1994; *Singh*, 1996, 1998]. Of note is that at larger $L$ values, only one of the field-aligned streams is typically observed, namely, the one from the closest ionosphere [*Olsen et al.*, 1987]. This result indicates that there is a field-aligned potential that repels the plasma from the conjugate hemisphere, probably due to the enhanced density and anisotropy in the equatorial region. A final population to consider is the ring current, which is enhanced simultaneously with the depletion of the thermal plasma [*Fok et al.*, 1995; *Jordanova et al.*, 1996].

The present study is an application of a time-dependent, field-aligned kinetic transport model to early stage plasmaspheric refilling, with the inclusion of self-consistent Coulomb collisions and parallel electric fields. It focuses on $H^+$ refilling with a given ionospheric outflow, concentrating on the magnetospheric processes contributing to populating the geomagnetic trap. The influences of each process are investigated, and the results are compared with previous model and observational studies. The influence of the observed hot plasma populations is also taken into account, and these effects are examined in detail. The necessity of a kinetic model for early stage plasmaspheric refilling is also evaluated here.

[1]Space Physics Research Laboratory, University of Michigan, Ann Arbor
[2]Physics Department and Geophysical Institute, University of Alaska Fairbanks
[3]Space Sciences Laboratory, NASA Marshall Space Flight Center, Huntsville, Alabama



Paper number 1999JA900104.
0148-0227/99/1999JA900104$09.00

## 2. The Model

The model to be used in this study was developed for superthermal electron transport in the ionosphere and plasmasphere (along a single flux tube) to investigate the refilling and depletion timescales of the trapped zone and the effects of these particles on ion refilling [e.g., *Khazanov et al.*, 1993; *Khazanov and Liemohn*, 1995; *Liemohn et al.*, 1997]. It has now been modified to calculate the ion distribution function,

still using the linearized Fokker-Planck Coulomb collision operator, but now taking the background species from the previous time step simulation results for a nonlinear solution. It solves the time-dependent, gyration-averaged kinetic equation for a plasma species' phase-space flux distribution $\phi(t, s, E, \mu_0)$, where the particle velocity $v$ has been converted to energy $E$ and the particle pitch angle $\alpha$ has been transformed into $\mu_0$, the cosine of its equatorial plane value (see *Khazanov et al.* [1993] for further details of this transformation). In these variables (time, field-aligned distance, energy, and equatorial pitch angle, respectively), $\phi$ is a slowly varying function of $s$, and numerical diffusion is greatly reduced. The flux function is related to the distribution function $f$ by $\phi=2Ef/m^2$. In these variables, the kinetic equation can be written in the form

$$\frac{\beta}{\sqrt{E}}\frac{\partial\phi}{\partial t}+\mu\frac{\partial\phi}{\partial s}-\frac{1-\mu^2}{2}\left(\frac{1}{B}\frac{\partial B}{\partial s}-\frac{F_{\parallel}}{E}\right)\frac{\partial\phi}{\partial\mu}+EF_{\parallel}\mu\frac{\partial}{\partial E}\left(\frac{\phi}{E}\right)=Q+\bar{S} \tag{1}$$

where $\beta=\sqrt{m/2}=7.19\times10^{-7}$ $\mathrm{eV^{1/2}cm/s}$ for $H^+$; $F_{\parallel}$ includes all parallel forces acting on the plasma species, particularly the self-consistent electric field; and $\bar{S}$ represents the collisional terms, which is the Coulomb collision operator in this study. Because the low-altitude boundary is chosen to be above the thermosphere (at 1000 km), atmospheric interactions can be neglected. The collision term can be written as

$$\bar{S}=\bar{S}_{CC}=A\sum_{\alpha}n_{\alpha}\left\{2\frac{\partial}{\partial E}\left[\frac{G_{\alpha}}{T_{\alpha}}\phi+G_{\alpha}E\frac{\partial}{\partial E}\left(\frac{\phi}{E}\right)\right]+\frac{\Phi_{\alpha}-G_{\alpha}}{4E^2}\frac{B_0\mu}{B\mu_0}\frac{\partial}{\partial\mu_0}\left[\frac{\mu}{\mu_0}\left(1-\mu_0^2\right)\frac{\partial\phi}{\partial\mu_0}\right]\right\} \tag{2}$$

In (2), $\Phi_{\alpha}$ is the error function with argument $x=v/u_{\alpha}$, where $u_{\alpha}=(k_BT_{\alpha}/m_{\alpha})^{1/2}$ is the thermal speed of species $\alpha$; and $G_{\alpha}$ has the same argument and is defined as

$$G_{\alpha}=G(x)=\frac{\Phi(x)}{2x^2}-\frac{\exp\left(-x^2\right)}{x\sqrt{\pi}}$$

Note that the sum over plasma species includes the ion population being calculated by the kinetic equation ($H^+$), whose thermal parameters will be taken from the previous time step. No terms in (2) are neglected (that is, pitch angle and energy diffusion are included in the calculation).

The kinetic equation is solved by replacing the derivatives with a combination of first- and second-order discrete differences and advancing the solution on a predefined grid in phase space. It uses a time-splitting technique to allow for the solution of each derivative separately. The altitude domain extends from 1000 km in one ionosphere through the plasmasphere to 1000 km in the conjugate ionosphere with 60 grid points throughout. And the equatorial pitch angle grid takes into account the changing magnetic field, starting with 5 points and adding a grid point with each altitude step. The energy grid has 45 points ranging from 0.025 eV up to 12 eV, with a geometrically increasing step size. The time step was chosen to be 3 s and ran for 4 hours of simulation time. At each time step, the first few moments of the distribution are calculated at each spatial location,

$$n=\int_{\infty}d^3v f=\sqrt{2m}\pi\int_{-1}^{1}d\mu\int_{0}^{\infty}\frac{\phi}{\sqrt{E}}dE \tag{3}$$

$$u=\frac{1}{n}\int_{\infty}d^3v v_{\parallel}f=\frac{2\pi}{n}\int_{-1}^{1}\mu d\mu\int_{0}^{\infty}\phi dE \tag{4}$$

$$T_{\parallel}=\frac{m}{n}\int_{\infty}d^3v\left(v_{\parallel}-u\right)^2f=\frac{2\sqrt{2m}\pi}{n}\int_{-1}^{1}\mu^2d\mu\int_{0}^{\infty}\sqrt{E}\phi dE-mu^2 \tag{5}$$

$$T_{\perp}=\frac{m}{2n}\int_{\infty}d^3v v_{\perp}^2f=\frac{\sqrt{2m}\pi}{n}\int_{-1}^{1}\left(1-\mu^2\right)d\mu\int_{0}^{\infty}\sqrt{E}\phi dE \tag{6}$$

The total temperature is given by $T=(2T_{\perp}+T_{\parallel})/3$. Moments for the refilling streams ($\mu>0$ and $\mu<0$) are also computed by splitting the $\mu$ integrals in half to yield values for the two velocity-space hemispheres.

The initial condition was chosen to represent a depleted flux tube. It is assumed that the initial distribution is a stationary, isotropic Maxwellian with a thermal electron density profile of $n(s)=n(s_1)(B(s)/B(s_1))^{\alpha}$, where the subscript "1" refers to the low-altitude boundary (1000 km) and $\alpha$ is determined to match a specified equatorial density. The electron temperature is assumed to be isothermal, so $T(s)=T(s_1)$. The values at $s_1$ for thermal electrons are $n=10^4$ $\mathrm{cm^{-3}}$ and $T=0.3$ eV, with 80% $O^+$ and 20% $H^+$ present, and the equatorial electron density is 1 $\mathrm{cm^{-3}}$, with 20% $O^+$ and 80% $H^+$. This initially high concentration is justified by the charge exchange of the geocorona with energetic $O^+$ ring current ions, which typically have densities of several to tens per cubic centimeter in the inner magnetosphere during a storm and is thus capable of maintaining this population at this level. The boundary condition during the simulation holds the upwardly injected Maxwellian $H^+$ distribution fixed, but the downward flowing stream is calculated. The net flux at the boundary is therefore variable but usually comparable to $10^8$ $\mathrm{cm^{-2}\ s^{-1}}$, a reasonable refilling flux [cf. *Chappell et al.*, 1970; *Schulz and Koons*, 1972; *Rasmussen et al.*, 1993]. The refilling is performed along an $L=4$ field line, with symmetric boundary conditions at the conjugate footpoints. As the simulations progress and the $H^+$ distribution changes, the electron density is allowed to vary to ensure quasi-neutrality everywhere, but the $O^+$ profile is held constant. This constraint is justified by the much longer refilling timescale of $O^+$ compared to $H^+$. Because of this quasi-neutrality assumption, the densities in the Coulomb collision terms are always self-consistent (to within a time step). The electron temperature is calculated using the thermal electron energy equation, yielding a temperature profile given by [*Khazanov et al.*, 1997a]

$$T_e^{7/2}(s)=T_{e1}^{7/2}+\frac{7}{2\kappa}\int_{s_1}^{s}B\left\{\frac{n_eu_e}{B}\left(\frac{5}{2}T_e+\frac{m_eu_e^2}{2}\right)-\left[\frac{n_eu_e}{B}\left(\frac{5}{2}T_e+\frac{m_eu_e^2}{2}\right)\right]_{s_0}+\left[\frac{\kappa T_e^{5/2}}{B}\frac{\partial T_e}{\partial s}\right]_{s_0}+e\left(\Delta\phi_{\parallel}^{s_0}-\Delta\phi_{\parallel}\right)\frac{n_eu_e}{B}\right\}ds \tag{7}$$

where $\kappa$ is the thermal conductivity coefficient, with a value of $7.7\times10^5$ $(\mathrm{cm\ s\ eV^{5/2}})^{-1}$ used here, and $\Delta\phi_{\parallel}$ is the potential difference along the field line (related to $F_{\parallel}$ in (1)). The thermal electron flux ($n_eu_e$) is found from the currentless condition. Additionally, some simulations use the calculated $H^+$ temperature in the Coulomb collisions from the previous time step, while others use the electron temperature instead. This differ-

ence in the background $H^+$ (the values used in (2)) will be discussed below.

Using these values, the field-aligned force term is calculated from the electron momentum equation [cf. *Liemohn et al.*, 1997]

$$F_{\parallel} = eE_{\parallel} \equiv -\frac{1}{n_e}\frac{\partial(n_e T_e)}{\partial s} \tag{8}$$

which is used in (1). Note that while the full momentum equation is used in the calculation, the simplified form is shown here to stress the dominant term in the equation. Because $n_e$ is updated every time step, this is a self-consistent electric field. Some simulations will use this definition for $F_{\parallel}$ and others will assume it to be zero, and the difference will be examined.

## 3. Results

The purpose of this study is to examine the effects of nonlinear self-consistency on early stage plasmaspheric ion refilling and how this relates to hot plasma influences on this process. Before we proceed, though, a baseline result without self-consistency will be discussed. In this simulation the "background" $H^+$ population in the Coulomb collision terms uses $T_e$ instead of the calculated $T_{H^+}$, and $F_{\parallel}$ is fixed at zero everywhere. Figure 1 shows flux distribution functions (in units of $cm^{-2}$ $s^{-1}$ $eV^{-1}$ $sr^{-1}$) at five spatial locations (evenly spaced along half of the field line) for two stages of the refilling process: $t$=15 min (very early stage) and 4 hours (approaching later stage). The two streams are clearly seen at the higher altitudes, although they are less distinct at lower altitudes. However, even at 4560 km, the beam is shifted off $v_{\parallel}$=0, especially at 15 min but even at 4 hours. Also seen at 15 min is the source cone bulge in the contours, naturally stronger in the positive flow direction because these particles are closer to their source. Source cone refers to the region of velocity space that maps (collisionlessly) to the ionospheric boundaries, and is exactly analogous to the loss cone present in energetic populations of magnetospheric origin.

Moments of these distributions are shown in Figure 2. These are stream moments, taken for $v_{\parallel}$>0 ($\mu$>0) along the entire field line. Note that because the simulation is spatially symmetric, there is an equal and oppositely directed stream flowing from the southern to the northern ionosphere. The various curves in the subplots are at t=0, 3 min, 15 min, 30 min, 1 hour, and 4 hours of simulation time. As the refilling progresses, the stream density first shows depletion in the latter half of the flux tube, then an increase starting from the source ionosphere and sweeping through the flux tube. The bulk flow of the stream is initially the flow from a half-Maxwellian, but quickly increases to 10 km $s^{-1}$ before settling near 8 km $s^{-1}$ along most of the field line. Keep in mind that these are moments taken over only half of the distribution, and thus must be cautiously considered in comparison with Figure 1. Due to the counterstreaming beam structure in Figure 1, it is thought that these velocities are close to the actual flow speeds of the streams and not an artifact of heating (although the increased spread at lower energies evident in Figure 1 does influence these moment calculations). Also note that newly injected ionospheric protons are not part of the velocity enhancement near (or beyond) the equatorial plane in the early stages of refilling; this velocity is from the initial plasma flowing along the field line and, for the most part, has a small

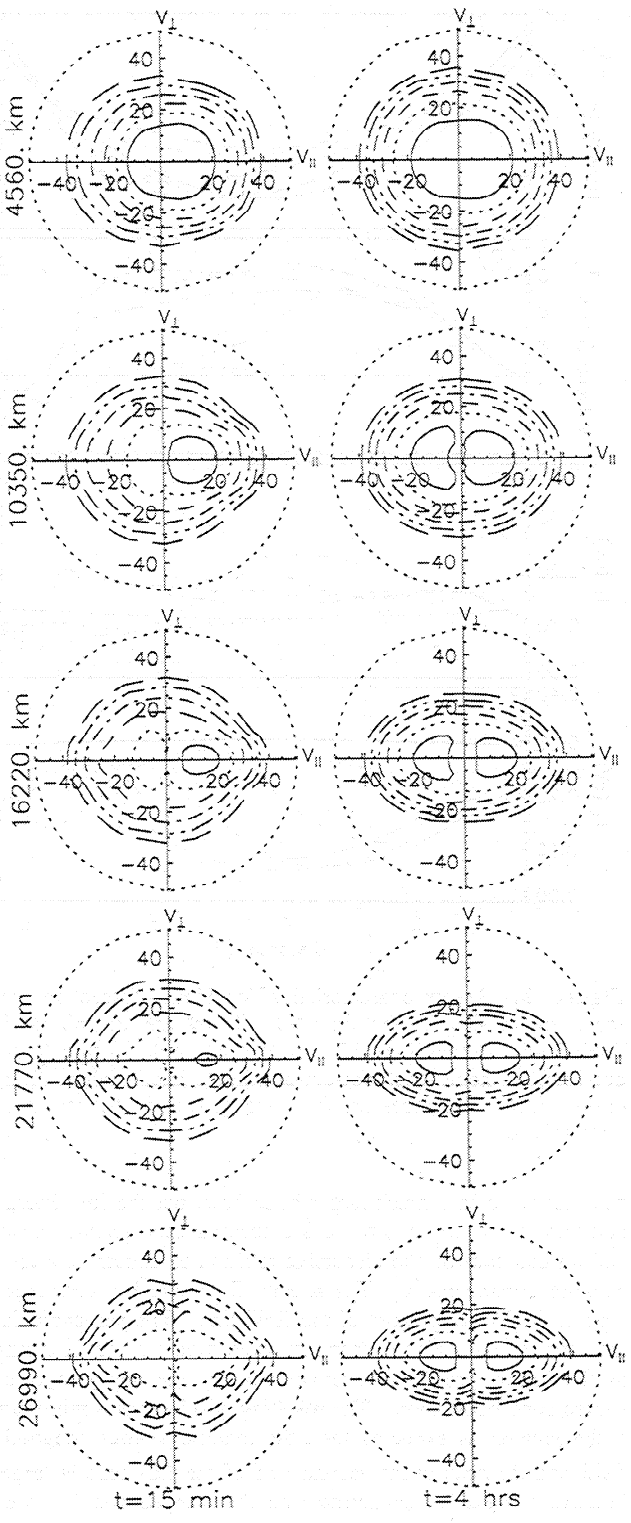


**Figure 1.** Flux distributions at five spatial points for Sim. 1 at $t$=15 min and 4 hours. The contours are spaced 1.5 orders of magnitude apart, starting with the solid curve at $10^6$ $cm^{-2}$ $s^{-1}$ $eV^{-1}$ $sr^{-1}$. The velocities are given in km/s, and the dotted circle at the outer velocity indicates the upper energy boundary of the simulations.

density associated with it. The large increase in $T_{\parallel}$ in the second half of the field line is due to the more energetic particles of the refilling flow passing through this region before the less energetic particles have made it this far. This might have

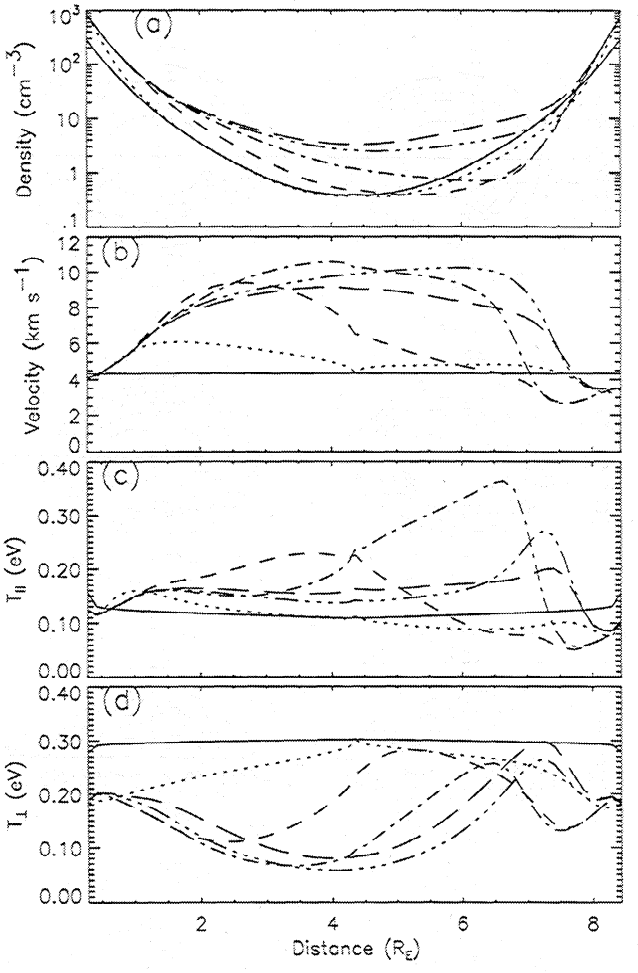


**Figure 2.** Stream characteristics for Sim. 1 based on moments of the distribution for $v_{\parallel}>0$. Times are are $t$=0 (solid line), 3 min (dotted line), 15 min (dashed line), 30 min (dash-dot line), 1 hour (dash-dot-dot-dot line), and 4 hours (long dashed line). Distances are from the ground in the northern hemisphere.

been reflected in a much larger bulk flow, but the low-energy particles of the initial profile are keeping this quantity down and instead causing the dispersive refilling to appear as a temperature enhancement. The stream $T_{\parallel}$ eventually converges near 0.18 eV along most of the field line. The perpendicular temperature has a sudden drop that sweeps across the field line as the initial profile is overwhelmed by the newly injected source cone population. The resulting profile has a minimum at the equator, as expected from the inhomogeneous magnetic field, and the peak in the second half of the flux tube is larger because of particles scattering into the trapped zone as they traverse the plasmasphere. It should be noted that the thermal electron temperature is nearly constant along the field line, dropping from the 0.3 eV boundary condition at 1000 km to 0.29 eV at the equatorial plane. This is because the thermal electron flows along the field line are balancing the ion flows, resulting in a very small $u_e$ value. More about this case is discussed as it is compared to other simulations below.

### 3.1. Influences of Self-Consistency

To illustrate the effects of self-consistent Coulomb collisions and polarization electric fields, several simulations were performed. These simulations are listed in Table 1. Sim. 1 is the run presented above, while Sims. 2-7 have some process changed or include one or both of the self-consistent processes.

To examine the effects of self-consistent Coulomb collisions on early stage plasmaspheric refilling, the time development of the equatorial $H^+$ density (both streams included) is shown in Figure 3 for Sims. 1-5. Sims. 1, 4, and 5 are all non-self-consistent calculations (that is, imposed $H^+$ temperatures used in (2) for the $H^+$ scattering target population, hereafter referred to as the background $H^+$), just with different proton temperatures in the collision terms. There is a clear increase in density (mostly in the source cone) with the temperature of the background $H^+$. This is believed to be because the higher temperatures are less efficient at removing particles from the source cone as the particles traverse the plasmasphere. Sim. 2 is a self-consistent calculation, with the background $H^+$ temperature in the Coulomb operator obtained from a single fit to the resulting distribution function at each altitude (integrate in (3)-(6) over all $\mu$), while Sim. 3 is a self-consistent calculation with a two-stream fit from the previous time step results (split the integrals in (3)-(6) at $\mu$=0). It is seen that the Sim. 3 results are higher than the Sim. 2 densities, as expected from the better nonlinear representation.

To further examine this influence, Figure 4 compares the $H^+$ temperature profiles for Sim. 1 and Sim. 2 at several times. Figure 4a shows the temperatures used in the collision operator, while Figures 4b and 4c show the Sim. 2 parallel and perpendicular temperatures of refilling ions. The self-consistent temperature starts out lower than the assumed temperature for most of the field line, goes through an increase near the equator, and then this region cools a bit while the rest of the field line increases. The equatorial plane temperature is largely governed by the parallel temperature, as seen in Figure 4b, and the decrease in the later stage is from the relaxing of the counterstreaming beams from the conjugate ionospheres. Lower down on the field line the total temperature is governed by the perpendicular temperature which shows a steady increase in the later stage as particles scatter into the trapped zone. The decrease during the early stage is from the replacement of the initial condition with the streaming plasma.

The inclusion of a self-consistent polarization electric field has a very noticeable effect on the results. The stream densities and perpendicular temperatures for Sim. 1 and Sim. 6 at $t$=18 min and 4 hours are shown in Figure 5. Here it is seen that the electric field acts to rapidly deplete the initial condition in the plasmasphere, yet also increases the refilling flow from the ionosphere. Another effect is a large increase in the

**Table 1.** Simulation Characteristics

| Simulation | $F_{\parallel}$ | $T_{H^+}$ Hot Populations |
|---|---|---|
| Sim. 1 | =0 | 0.3 eV constant, isothermal |
| Sim. 2 | =0 | S-C, single-stream fit |
| Sim. 3 | =0 | S-C, two-stream fit |
| Sim. 4 | =0 | 0.5 eV constant, isothermal |
| Sim. 5 | =0 | 0.05 eV constant, isothermal |
| Sim. 6 | S-C | 0.3 eV constant, isothermal |
| Sim. 7 | S-C | S-C, single-stream fit |

S-C, self-consistent.

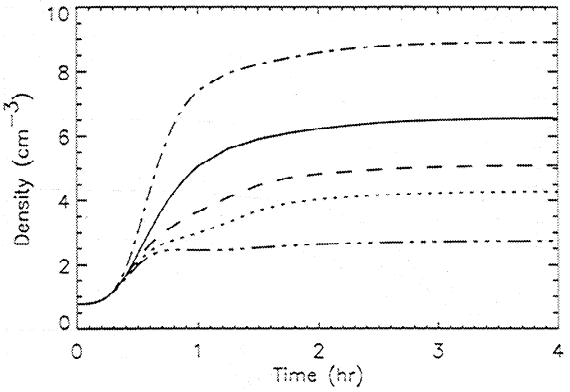


**Figure 3.** Equatorial densities for Sim. 1 (solid line), Sim. 2 (dotted line), Sim. 3 (dashed line), Sim. 4 (dash-dotted line), and Sim. 5 (dash-dot-dot-dot line) as a function of simulation time.

stream bulk speed, up to a maximum of 18 km s$^{-1}$ during the early stage of refilling and a late stage profile with a slight peak up to 15 km s$^{-1}$ at the equator. The stream $T_{\parallel}$ is also enhanced, with a peak up to 0.75 eV at 24 min and a late stage level around 0.25 eV along the field line. The spatial profiles of the electric field and electrostatic potential difference for Sim. 6 are shown in Figure 6. It is seen that the electric field never exceeds 0.25 μV/m, accumulating a potential drop of less than 2.6 V for the initial distribution and 1.8 V at 4 hours. This potential drop directly corresponds to the increase in bulk flow of the ionospheric outflow streams. Notice that there is a significant drop in the electric field between 15 and 30 min at high altitudes. This is because of the initial front of ionospheric plasma passing through the flux tube. Once it reaches a point along the field line, the thermal electron density jumps up correspondingly and the electric field decreases.

Sim. 7 includes both of the self-consistent processes, and the result is essentially a combination of the two (that is, no unexpected nonlinear effects occur). Figure 7 shows the time development of the equatorial $H^+$ density (both streams included) for four of the simulations (1, 2, 6, and 7). There is a clear difference between the runs with and without a self-consistent $T_{H^+}$ (lower and higher, respectively) and also a clear difference between runs with and without a self-consistent $F_{\parallel}$ (higher and lower, respectively). Note that the simulations show a similar density increase after 2 hours of simulation, an increase of about 0.1 cm$^{-3}$/hour, except for Sim. 6, which rises faster (~0.3 cm$^{-3}$/hour) and also has the largest source cone density. This is expected because the collisional scattering into the trapped zone is directly proportional to the density of the scattering targets. The slight plateau in the Sim. 6 and Sim. 7 results from 30 to 90 min is from a changeover of the dominant refilling process: at first, $F_{\parallel}$ creates an enhanced field-aligned flow, and then later Coulomb scattering slowly refills the plasmaspheric trap. The sharpness of this rise is not seen in the results with $F_{\parallel}$=0 because the ionospheric flows

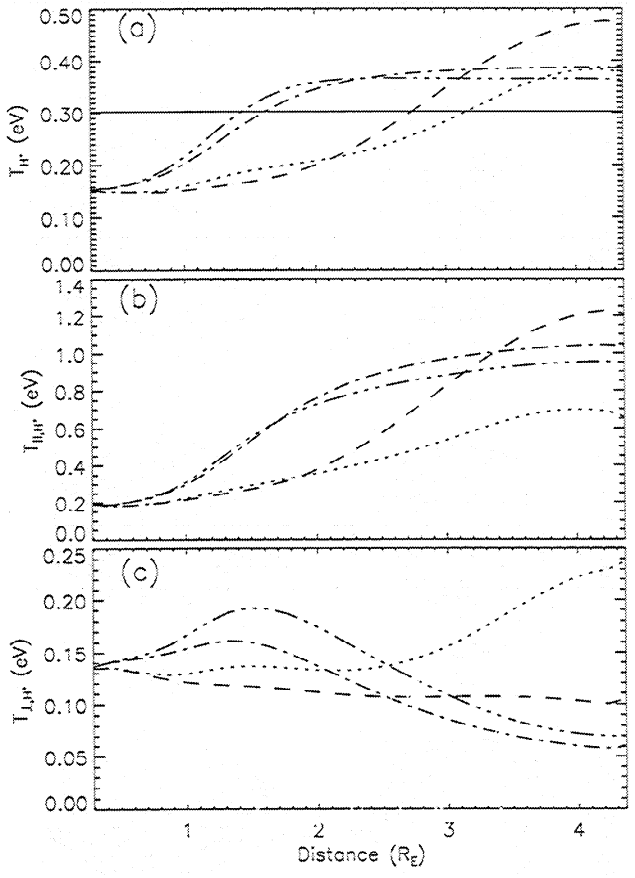


**Figure 4.** (a) $H^+$ temperature profiles used in the Coulomb collision operator for Sim. 1(solid line) and Sim. 2 at $t$=15 min (dotted line), 30 min (dashed line), 1 hour (dash-dot line), and 4 hours (dash-dot-dot-dot line). Sim. 1 is given, and Sim. 2 temperatures are calculated from the resulting distribution. Also plotted from Sim. 2 are single Maxwellian fit (b) parallel temperatures and (c) perpendicular temperatures.

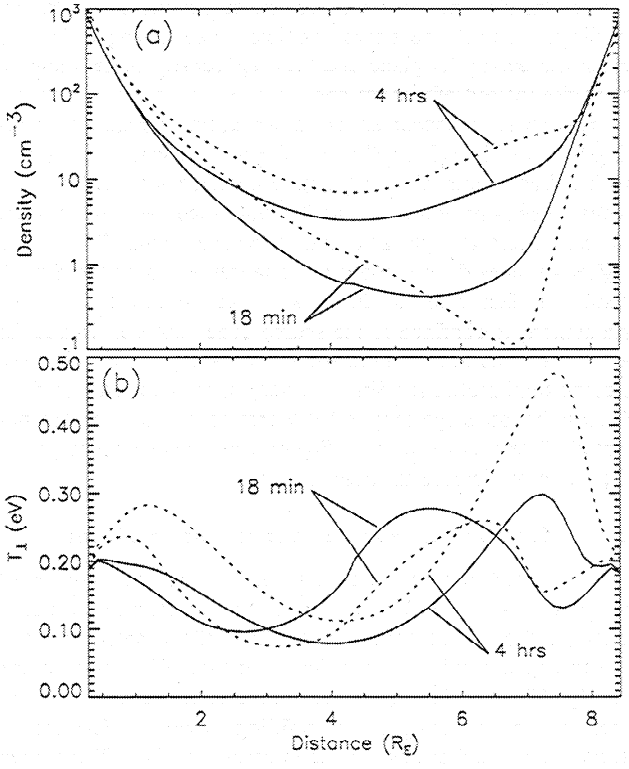


**Figure 5.** Stream ($v_{\parallel}$>0) density and perpendicular temperature for Sim. 1 (solid lines) and Sim. 6 (dotted lines) at $t$= 18 min and 4 hours, as indicated.

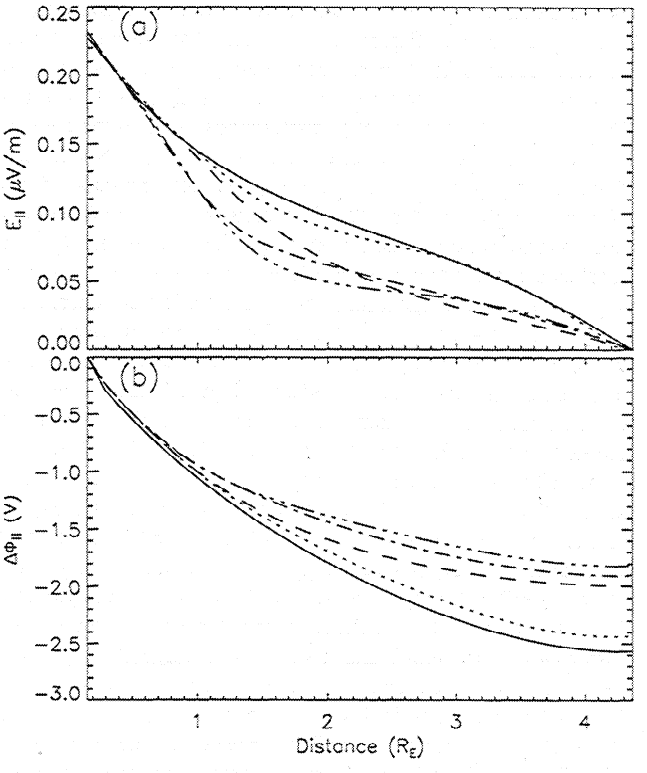


**Figure 6.** Electric field and electrostatic potential profiles for Sim. 6 at $t$=0 (solid lines), 15 min (dotted lines), 30 min (dashed lines), 1 hour (dash-dot lines), and 4 hours (dash-dot-dot-dot lines).

are not being accelerated. That is, $\Delta\phi_{||}>>T_{H^+}$, so in Sims. 6 and 7, even the slow particles are accelerated beyond 10 km/s, but in Sims. 1 and 2, the slower particles take a longer time to reach the equatorial plane and thus the density there shows a slow rise instead of a sharp one.

This initial enhancement is shown again in Figure 8, plotting flux functions from Sim. 1 and Sim. 7 at $t$=30 min. Along with a fairly isotropic temperature enhancement at low altitudes, there is an enhanced parallel flow speed and temperature for each beam at high altitudes. However, Sim. 7 $T_\perp$ at the higher altitudes do not show an enhancement over the Sim. 1 results. In fact, most of the density increase between the two simulations is confined to the source cone, and this is true for all of the simulations discussed in this study. Note that the electric field profile for Sim. 7 is very similar to that for Sim. 6, only the late stage drop is 1.9 V instead of 1.8 V, so the potential differences shown in Figure 6 can be used to interpret the velocity increase in these results.

### 3.2. Hot Population Influences on Refilling

It is clear from the previous section that self-consistent temperatures in the Coulomb collision operator can reduce or enhance the source cone population while a self-consistent electric field provides a significant early-time boost to the refilling. These influences, however, are obtained with only the thermal plasma acting on the refilling process. Here the effects of hot populations on the thermal plasma refilling rates will be examined in the context of a self-consistent simulation. During geomagnetic disturbances, the ring current is enhanced well above its quiet-time levels [e.g., *DeForest and McIlwain*, 1971; *Ejiri et al.*, 1978; *Thomsen et al.*, 1998], and these hot populations coexist in the inner magnetosphere with the depleted thermal plasma densities. In addition to ring current ions, warm highly anisotropic ion populations also exist in the inner magnetosphere [e.g., *Horwitz et al.*, 1981; *Olsen et al.*, 1987, 1994]. These populations will influence the field-aligned electric field and contribute to the Coulomb interactions, thus altering the refilling rates of the thermal plasma.

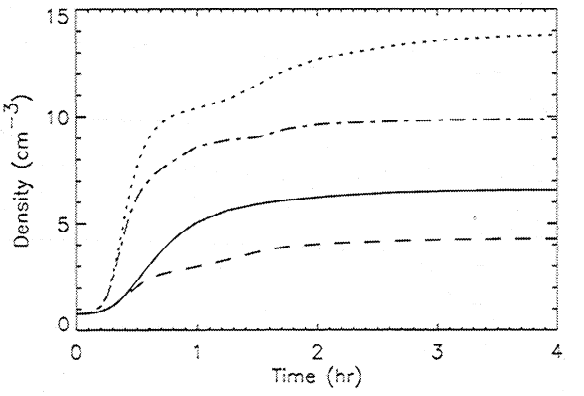


**Figure 7.** Equatorial plane $H^+$ densities (both streams) for Sim. 1 (solid line), Sim. 2 (dashed line), Sim. 6 (dotted line), and Sim. 7 (dash-dot line) as a function of simulation time.

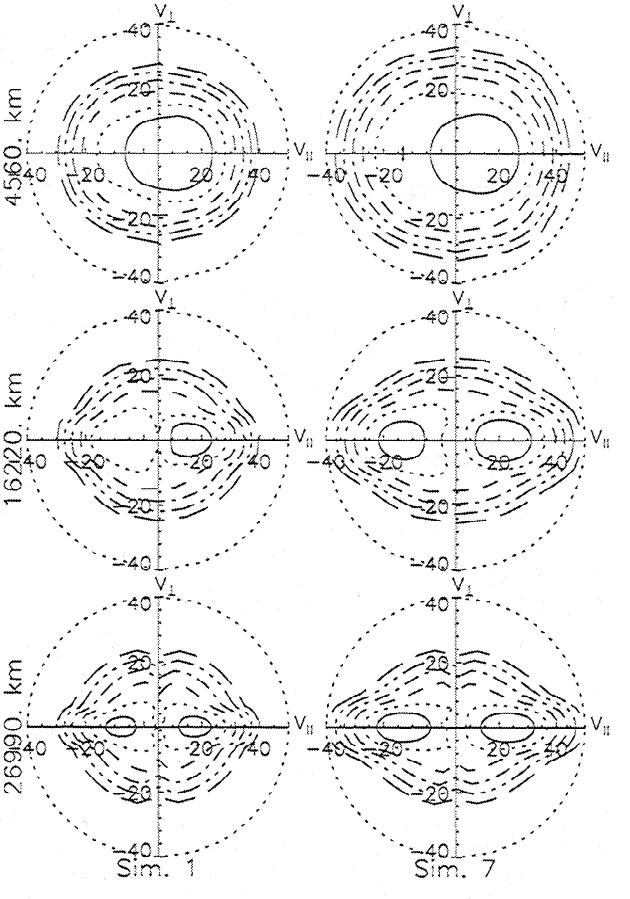


**Figure 8.** Flux distribution functions for Sim. 1 and Sim. 7 at $t$=30 min for three spatial points, as a function of $v_{||}$ and $v_\perp$ (in km/s).

These populations were included in several simulations: Sim. 8, Sim. 9, and Sim. 10. All are similar to Sim. 7, except that hot anisotropic plasma has been included as background populations. Table 2 details the characteristics of these energetic populations for the three runs. Sim. 8 included a moderate $H^+$ and $O^+$ ring current population with two bi-Maxwellian distributions each. The two distributions are needed to realistically depict the ring current velocity space function because ions near 10 keV undergo a stagnation on the nightside due to the competing drift processes, creating a minimum in the dayside distributions at this energy [*McIlwain*, 1972]. The parameters were chosen from a typical ring current simulation [*Jordanova et al.*, 1996; *Kozyra et al.*, 1998]. The second hot plasma effects simulation included a greatly enhanced ring current density, a phenomenon that occurs during large storms and superdense plasma sheet injections. The final simulation includes a warm pancake distribution similar to those described by *Olsen et al.* [1994]. These equatorial plane values are held constant throughout the simulations. This is a valid assumption considering that the typical time for ring current decay is a day or more.

These distributions are not limited to the equatorial plane, however. Their distribution along the field line is determined with a solution to Liouville's theorem of phase space mapping. While a rigorous approach would require calculating these distributions self-consistently with the polarization electric field influencing the thermal plasma [cf. *Liemohn and Khazanov*, 1998; *Khazanov et al.*, 1998], that field is much smaller than the temperatures of these populations and therefore has a negligible effect on the field line profiles of these populations. In this limit, Liouville's theorem yields a density profile along the field line of the form

$$n(s)=\frac{n_0 B(s)}{B(s)A-B_0(A-1)} \tag{9}$$

where the "0" subscript denotes values at the equatorial plane and $A=T_\perp/T_\parallel$ is also defined at the equator. This profile has $n_0$ at the equator (which is $n_{eq}$ from Table 2) but does not leave the desired zero density at the ionospheric boundaries. Instead it leaves

$$n_1=\frac{n_0 B_1}{B_1 A-B_0(A-1)} \tag{10}$$

To achieve zero density at the footpoints, the loss cone density given by (10) must be subtracted out of (9). This subtraction yields

$$n(s)=\frac{n_0 B_0\left(B_1-B(s)\right)(A-1)}{\left[AB(s)-B_0(A-1)\right]\left[AB_1-B_0(A-1)\right]} \tag{11}$$

This, however, gives something less than $n_0$ at the equator, and so $n_0$ is redefined according to (11) at the equator,

$$n_0=n_{eq}\frac{AB_1-B_0(A-1)}{\left(B_1-B_0\right)(A-1)} \tag{12}$$

where $n_{eq}$ is from Table 2. Using (12) in (11) yields

$$n(s)=\frac{n_{eq}B_0\left(B_1-B(s)\right)}{\left(B_1-B_0\right)\left[AB(s)-B_0(A-1)\right]} \tag{13}$$

which has $n_{eq}$ at the equator and $n$=0 at the ionospheric boundary. Because of the large anisotropies of these populations, the densities fall off rapidly away from the equator. Additional thermal electrons along the field line balance their densities to maintain quasi-neutrality. Because of this choice of field line profile, there is no field-aligned flux from these hot populations, and therefore the flux balance equation still consists of only the thermal electrons and ions. Consequently, the thermal electron temperature profile remains nearly isothermal along the flux tube.

These hot populations are then used to alter the $n_e$ field line profile and thus change the electric field. They are also included in the Coulomb collision operator as background populations for further interaction with the thermal $H^+$.

It is expected that these equatorially confined hot populations will create a thermal electron density enhancement along the field line, thus reversing the direction of the electric field. Profiles of the field-aligned potential differences for Sims. 7-10 are shown in Figure 9. Note the slightly different scales for the four subplots. Figure 9a is quite similar to Figure 6b, with a net drop of 1.9 V at the later stage refilling. Because of the presence of the hot plasma, Figures 9b - 9d have nonmonotonic potential distributions at all times, most dramatically at $t$=0. The three runs have progressively larger potential barriers at the equatorial region due to the increase in thermal plasma density to balance the charge of the hot ions. It can be seen, though, that this barrier is much smaller than the drop from the thermal plasma profile.

These potential distributions have only a slight effect on the refilling of the thermal ions. Figure 10 shows the equatorial densities of the four simulations for the first few hours. Figure 10a shows the $H^+$ densities during the first 30 min of the runs. The density initially decreases as the initial condition ions are quickly evacuated from the equatorial region faster than they can flow up from the ionospheres. The density climbs after this, however, as the ionospheric outflows reach this altitude and start populating the region. Figure 10b shows a very interesting result: the refilling density increases with increasing hot plasma density. This is because the particles are slowed down more as they pass the equatorial region,

**Table 2.** Hot Population Characteristics

| | $H^+_{RC1}$ | $H^+_{RC2}$ | $O^+_{RC1}$ | $O^+_{RC2}$ | $H^+_{WP}$ |
|---|---|---|---|---|---|
| | *Sim. 8 Populations:* $\Sigma n_{eq}$=7.5 $cm^{-3}$ | | | | |
| $n_{eq}$, $cm^{-3}$ | 0.5 | 1.0 | 3.0 | 2.5 | -- |
| $T_\perp$, eV | 5000 | 50,000 | 5000 | 50,000 | |
| $T_\perp/T_\parallel$ | 5 | 5 | 5 | 5 | |
| $m/m_p$ | 1 | 1 | 16 | 16 | |
| | *Sim. 9 Populations:* $\Sigma n_{eq}$=25 $cm^{-3}$ | | | | |
| $n_{eq}$, $cm^{-3}$ | 1.0 | 4.0 | 10. | 10. | -- |
| $T_\perp$, eV | 5000 | 50,000 | 5000 | 50,000 | |
| $T_\perp/T_\parallel$ | 5 | 5 | 5 | 5 | |
| $m/m_p$ | 1 | 1 | 16 | 16 | |
| | *Sim. 10 Populations:* $\Sigma n_{eq}$=45 $cm^{-3}$ | | | | |
| $n_{eq}$, $cm^{-3}$ | 1.0 | 4.0 | 10. | 10. | 20. |
| $T_\perp$, eV | 5000 | 50,000 | 5000 | 50,000 | 25. |
| $T_\perp/T_\parallel$ | 5 | 5 | 5 | 5 | 20 |
| $m/m_p$ | 1 | 1 | 16 | 16 | 1 |

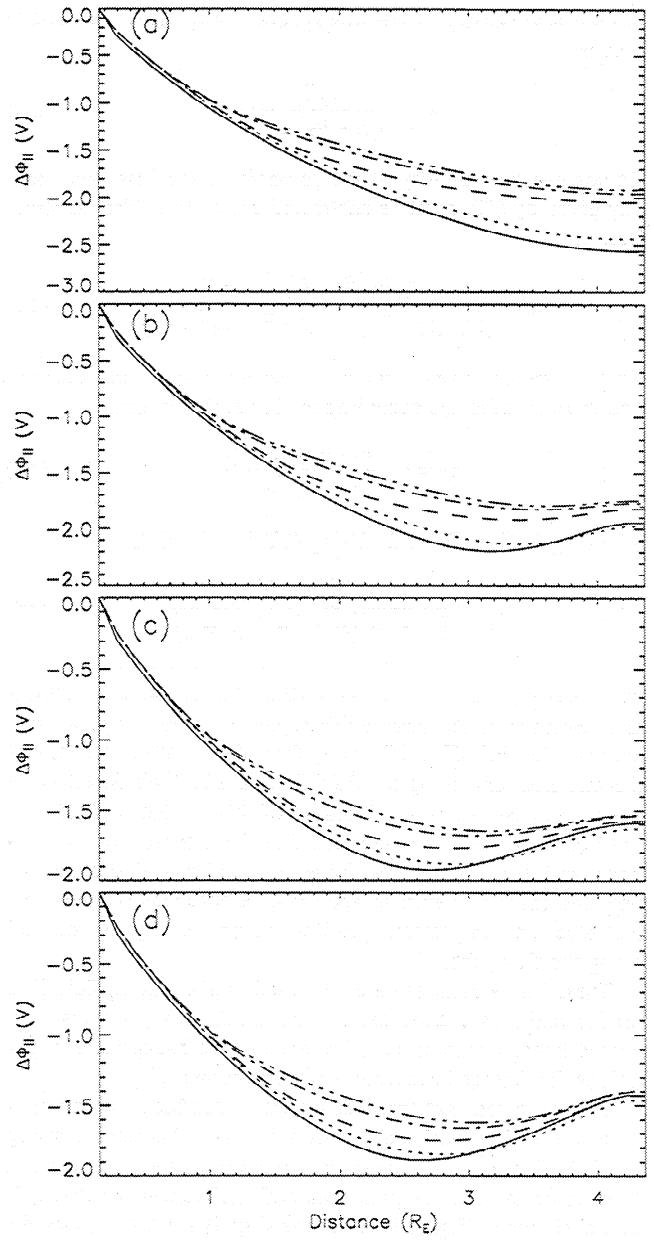


**Figure 9.** Electrostatic potential profiles for (a) Sim. 7, (b) Sim. 8, (c) Sim. 9, and (d) Sim. 10 at $t$=0 (solid lines), 15 min (dotted lines), 30 min (dashed lines), 1 hour (dash-dot lines), and 4 hours (dash-dot-dot-dot lines).

allowing more buildup not only in the source cone but also in the trapped zone due to increased scattering by the enhanced thermal electron population. Also, once again a plateau is seen in the density of all four simulations near 1 hour as the refilling process changes from field-aligned flow dominated (early stage) to scattering dominated (late stage).

Figure 11 shows stream quantities along the field line from the four simulations. Figure 11a shows the bulk flows after 4 hours of refilling, revealing the decrease in flow speed in the simulations with larger hot populations. This is a direct result of the reversed electric field seen in Figure 9. The stream velocity never reaches zero, however, because the potential barrier from the added populations is smaller than the potential drop from the thermal plasma profile. Figures 11b and 11c show the stream $T_\perp$ at 15 min and 4 hours, respectively. At 15 min, the initial front of the refilling stream is still propagating across the plasmasphere, and so the first half of the distribution is identical for the four simulations. The latter half of the flux tube shows enhancements in the stream $T_\perp$ with increasing hot plasma density. This can be explained as an increase in the amount of initial profile plasma being swept away from the equatorial region, enhancing the trapped zone fluxes at these altitudes. After 4 hours, the profiles look very similar, with only a slight increase in $T_\perp$ with hot plasma density. This is due to the increased density in the thermal electrons providing additional scattering to the thermal ions and contributing to the trapped zone fluxes. This is a good measure of the influence of the electrons on ion scattering into the trapped zone: even though the density increases by 7.5, 25, and 45 cm$^{-3}$ for the three hot plasma simulations, the $H^+$ $T_\perp$ is affected only marginally.

Finally, the initial stages of the refilling ($t$=15 min) are shown in the flux distribution functions of Figure 12 for Sim. 7 and Sim. 10. The two runs have nearly identical results in the low-altitude range, but a clear depletion is seen near the equatorial plane. An interesting feature in these results is the increase in the downward fluxes for Sim. 10 at the midrange altitude presented. This is from the increased removal of the initial profile ions from the equatorial region by the reversed electric field.

## 4. Discussion

One question to consider from these results is if it is worth the extra computational effort to perform the kinetic simulation rather than using a hydrodynamic model. Because hydrodynamic approaches approximate the velocity space function

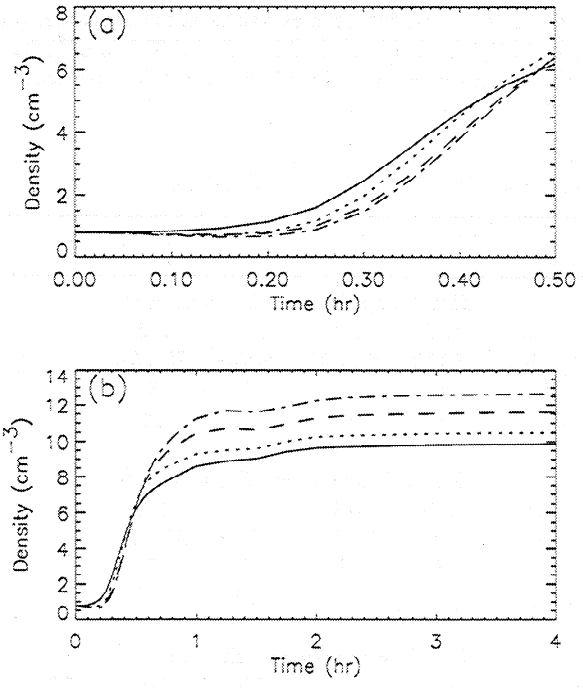


**Figure 10.** Equatorial plane $H^+$ densities from Sim. 7 (solid line), Sim. 8 (dotted line), Sim. 9 (dashed line), and Sim. 10 (dash-dot line) as a function of simulation time for (a) the first 30 min and (b) the first 4 hours.

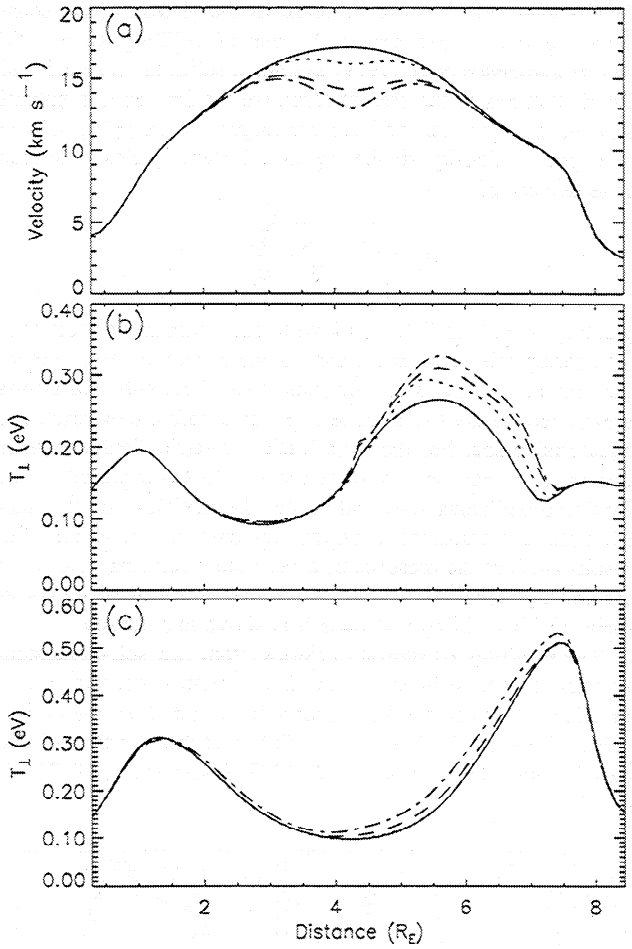


**Figure 11.** Stream ($v_\parallel$>0) characteristics for Sim. 7 (solid line), Sim. 8 (dotted line), Sim. 9 (dashed line), and Sim. 10 (dash-dotted line) showing (a) velocities at 4 hours, (b) $T_\perp$ at 15 min, and (c) $T_\perp$ at 4 hours.

with an equilibrium distribution, an answer can be obtained by comparing the resulting distributions to Maxwellian fits. This comparison is somewhat qualitative, however, because hydrodynamic approaches would not necessarily calculate the same moments as a full kinetic approach such as this, particularly if the distribution is far from a Maxwellian. Figures 13 and 14 show such a comparison for Sim. 7 and Sim. 10, respectively. These show only the field-aligned components of the calculated fluxes (that is, pitch angles of 0° and 180° only), but this yields an indication of the quality of the comparison. In these figures the left column is at $t$=15 min and the right column is at $t$=1 hour, both times during the early stage refilling process before the simulations reached the slow trapped zone refilling stage. Integrals of the velocity space distributions using (3)-(6) were calculated, once over the entire range of $\mu$ and again as two separate moments by splitting this integral at $\mu$=0 (that is, calculating the moments from each hemispherical ion stream). These moments are shown in Figures 13 and 14 by using the calculated densities, velocities, and temperatures as the bulk values in various Maxwellian distribution "fits" to the simulated distributions: a full-velocity-space bi-Maxwellian; a full-velocity-space isotropic Maxwellian; a two-stream bi-Maxwellian; and a two-stream isotropic Maxwellian. The isotropic temperatures are found from the moments as $T=(T_\parallel+2T_\perp)/3$. These four fits are shown along with the calculated field-aligned fluxes from the kinetic model. It is seen that none of the fits are close for all of the plots shown, but some are quite close for individual spectra. The fits are less accurate at the higher altitudes, particularly the full-distribution Maxwellian fits. Another interesting feature is that the fits are better for Sim. 7 than for Sim. 10. The added complexity from the nonmonotonic potential difference forces the calculated distributions farther from a Maxwellian. It is also interesting that the Maxwellian fits are not systematically different from the calculated spectra. That is, sometimes they have a larger peak and smaller tail and other times the opposite. This makes it very difficult to try to estimate a correction factor to the Maxwellian fits because there is not a single explanation (such as increasing the tail). Keep in mind that these fits include the calculated drift speed to provide the appropriate offset to the Maxwellian distributions.

Because Maxwellian distributions are not good approximations to the refilling streams, it would appear that even the present technique of using these Maxwellian fits for the background populations for the next time step (our nonlinear approach) has room for improvement. Indeed, fitting these distributions with a more complicated distribution provides better feedback from the refilling streams. As noted above, the two-stream Maxwellian fit in the self-consistent Coulomb collisions had a higher source cone density than from the single

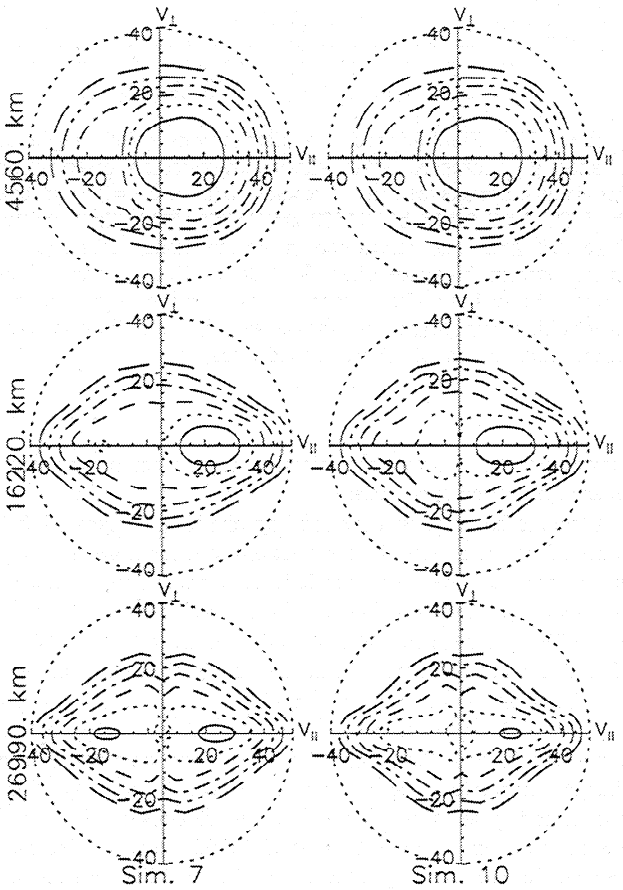


**Figure 12.** Flux distribution functions for Sim. 7 and Sim. 10 at 15 min for three spatial points, as a function of $v_\parallel$ and $v_\perp$ (in km/s).

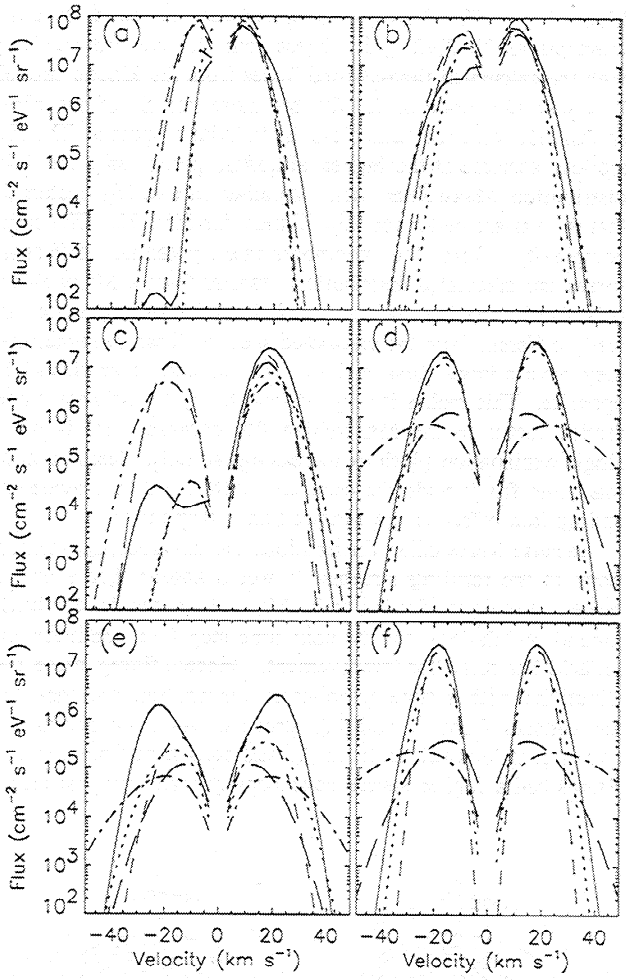


**Figure 13.** Field-aligned flux distributions (pitch angle of 0° and 180°) compared with various Maxwellian distribution fits from moments of Sim. 7 results at (a, c, e) $t$=15 min and (b, d, f) 1 hour for (a, b) $s$=4560 km, (c, d) 16,220 km, and (e, f) 26,990 km. The curves shown are the model results (solid lines), stream bi-Maxwellian fits (dotted lines), stream isotropic Maxwellian fits (dashed lines), full distribution bi-Maxwellian fits (dash-dot lines), and full distribution isotropic Maxwellian fits (long dashed lines).

Maxwellian fit. Further modification of this could further increase the source cone density.

It should be noted that the refilling rate is quite slow after 4 hours of refilling, with the distributions still far from isotropy in the trapped zone. This result is quite analogous to that of *Lawrence et al.* [1999]. They concluded that there are, in fact, two refilling timescales, a slow initial refilling rate of 0.6 to 12 cm$^{-3}$/d when Coulomb collisions are inefficient, followed by a faster rate of 10 to 50 cm$^{-3}$/d after some critical mass has built up in the plasmasphere to allow Coulomb collisions to more rapidly fill the trapped zone. They determined the changeover between these two rates to occur after a day of refilling, noting the similarity to the critical density of 10 cm$^{-3}$ for fast refilling in the *Wilson et al.* [1992] results. The present results are showing a third (zeroth?) refilling timescale: the initial front passing through the plasmasphere, filling the source cone with ionospheric plasma up to some initial level from which the *Lawrence et al.* [1999] "early stage" begins. This is seen in the results presented as the plateau in the equatorial density values around 1 hour of refilling time. Of course, *Lawrence et al.* [1999] examined refilling at $L$=6.6 and the simulations of the present study are for $L$=4, so it is natural that the densities shown here are larger. A mapping of the ionospheric density to the equatorial plane yields a source cone density of

$$n_0 = n_1\left(1-\sqrt{1-\frac{B_0}{B_1}}\right) \tag{14}$$

yielding $n_0 \approx 14$ cm$^{-3}$ for $L$=4 with our boundary conditions. Comparing this value to the early stage equatorial plane densities found in this study reveals that Coulomb collisions greatly reduce the source cone population before they reach the equatorial plane, but the polarization electric field enhances this back up near the undisturbed level. This is expected, since Coulomb collisions slow and scatter the particles but the electric field accelerates them and thus lessens this reduction. Our results confirm the presence of a very slow refilling rate when the density is below 10 cm$^{-3}$, as well as confirm the enhancement of this refilling rate once it is above this density.

The resulting equatorial densities from the self-consistent simulations are between 10 and 15 cm$^{-3}$ after 4 hours of refilling, fairly consistent with observations and other theoretical calculations of plasmaspheric refilling at this $L$ value [*Sojka and Wrenn*, 1985; *Wilson et al.*, 1992; *Miller et al.*, 1993]. It

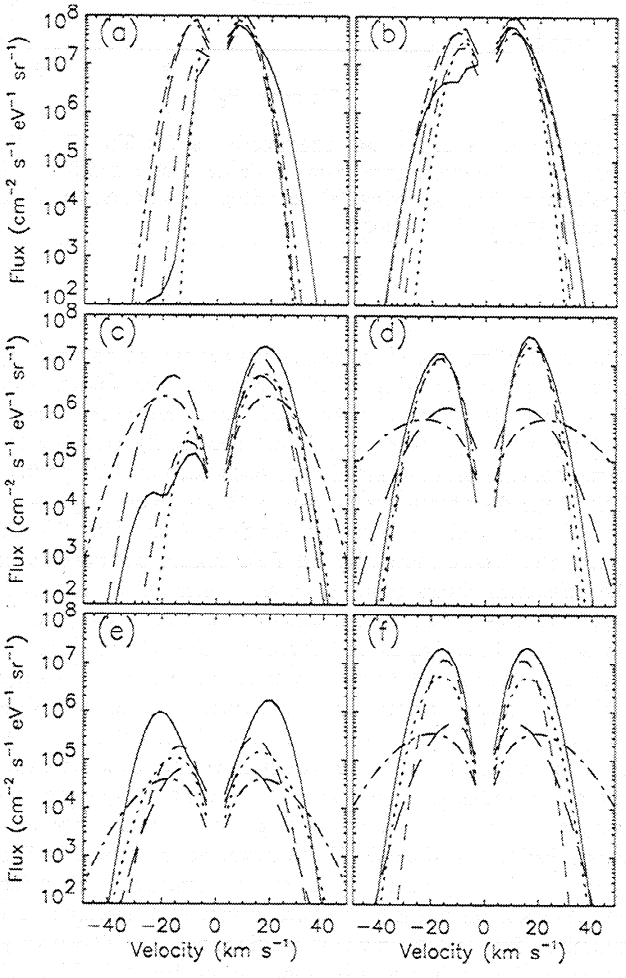


**Figure 14.** Same as Figure 13 but for Sim. 10.

is also quite consistent with refilling rates outside of the plasmasphere, such as those seen at geosynchronous orbit [e.g., *Wrenn et al.*, 1984; *Song et al.*, 1988]. Another observation of *Wrenn et al.* [1984] found that the source cone is broadened beyond that expected by adiabatic outflow. This is also a characteristic of the results shown in this study.

Some of the warm pancake distributions seen by *Olsen et al.* [1987] with Dynamics Explorer 1 in the outer plasmasphere were accompanied by unidirectional streams of cold ions. They concluded that the unidirectional nature of the refilling plasma was due to a potential barrier formed by the hot plasma, preventing the interhemispheric flows of cold ions. This was not reproduced in the present study, and in fact it was determined that the warm plasma does not create a sufficient potential barrier to prevent outflow streams from reaching the conjugate ionosphere. This could mean several things: there are other processes creating potential barriers near the apex of the field lines; the ionospheric outflows are far from symmetric, and so these potential distributions do not resemble those found in this study; or a more sophisticated field-aligned potential algorithm should be used in the calculation. It should be noted that other pancake distributions presented by *Olsen et al.* [1987] did have counterstreaming ion beams, analogous to the simulated refilling events discussed here.

## 5. Conclusions

A new approach to cold ion refilling of the plasmasphere has been used to examine the effects of self-consistency on the $H^+$ refilling rates. It was found that a self-consistent ion temperature in the Coulomb collision operator can increase or decrease the early stage refilling rate, depending on the choice of ion temperature in the static background simulations, while a self-consistent electric field increases the source cone density by more than a factor of 2. Investigations of the influence of anisotropic hot plasma populations on the refilling rates show that, after an initial decrease in density, there is a slight increase in the refilling rate due to these populations. This increase is caused by a slowing of the refilling streams near the equator due to the reversed electric field and also due to additional pitch angle scattering from the enhanced thermal electron density. It was also shown that the resulting distributions rarely resemble a Maxwellian, particularly at high altitudes.

It should be noted that this study included Coulomb interactions as the only collisional operator in the kinetic equation. Other processes could also be included, particularly the influence of plasma waves on the refilling rate. *Singh* [1998] has shown that scattering due to self-generated ion cyclotron waves increases the trapped zone density near the equator during the early stages of the refilling process, when the counterstreaming beams are unstable. There are other plasma waves that can also influence the cold ions, particularly lower-hybrid waves [e.g., *Olsen et al.*, 1987; *Khazanov et al.*, 1997b], which might also need to be considered in modeling plasmaspheric refilling. Inclusion of wave-particle interactions such as these is planned for the near future, as well as other modifications, such as a more rigorous inclusion of the hot populations in the $F_{\parallel}$ calculation using the method of *Liemohn and Khazanov* [1998]. A further modification planned for the near future is the incorporation of a more sophisticated background plasma calculation from the previous time step results to improve the self-consistent feedback from the streaming plasma.

**Acknowledgments.** This work was supported by NSF grants ATM-9711381, ATM-9710326, and ATM-9800830, and NASA grants NAG5-6976 and NAG5-4771. MWL held a National Research Council Postdoctoral Resident Research Associateship at NASA Marshall Space Flight Center while part of this work was performed.

Janet G. Luhmann thanks Howard G. Demars and another referee for their assistance in evaluating this paper.

## References

Banks, P. M., A. F. Nagy, and W. I. Axford, Dynamical behavior of thermal protons in the mid-latitude ionosphere and magnetosphere, *Planet. Space Sci., 19*, 1053, 1971.

Carpenter, D. L., and R. R. Anderson, An ISEE/whistler model of equatorial electron density in the magnetosphere, *J. Geophys. Res., 97*, 1097, 1992.

Chandler, M. O., and C. R. Chappell, Observations of the flow of $H^+$ and $He^+$ along magnetic field lines in the plasmasphere, *J. Geophys. Res., 91*, 8847, 1986.

Chappell, C. R., K. K. Harris, and G. W. Sharp, The morphology of the the bulge region of the plasmasphere, *J. Geophys. Res., 75*, 3848, 1970.

Curtis, S. A., Equatorial trapped plasmasphere ion distributions and transverse stochastic acceleration, *J. Geophys. Res., 90*, 1765, 1985.

DeForest, S. E., and C. E. McIlwain, Plasma clouds in the magnetosphere, *J. Geophys. Res., 76*, 3587, 1971.

Ejiri, M., R. A. Hoffman, and P. H. Smith, The convection electric field model for the magnetosphere based on Explorer 45 observations, *J. Geophys. Res., 83*, 4811, 1978.

Elphic, R. C., L. A. Weiss, M. F. Thomsen, D. J. McComas, and M. B. Moldwin, Evolution of plasmaspheric ions at geosynchronous orbit during times of high geomagnetic activity, *Geophys. Res. Lett., 23*, 2189, 1996.

Fok, M-C., T. E. Moore, J. U. Kozyra, G. C. Ho, and D. C. Hamilton, Three-dimensional ring current decay model, *J. Geophys. Res., 100*, 9619, 1995.

Guiter, S. M., and T. I. Gombosi, The role of high-speed plasma flows in plasmaspheric refilling, *J. Geophys. Res., 95*, 10,427, 1990.

Guiter, S. M., T. I. Gombosi, and C. E. Rasmussen, Two-stream modeling of plasmaspheric refilling, *J. Geophys. Res., 100*, 9519, 1995.

Horwitz, J. L., Core plasma in the magnetosphere, *Rev. Geophys., 25*, 579, 1987.

Horwitz, J. L., C. R. Baugher, C. R. Chappell, E. G. Shelley, and D. T. Young, Pancake pitch angle distributions in warm ions observed with ISEE 1, *J. Geophys. Res., 86*, 3311, 1981.

Jordanova, V. K., L. M. Kistler, J. U. Kozyra, G. V. Khazanov, and A. F. Nagy, Collisional losses in the ring current, *J. Geophys. Res., 101*, 111, 1996.

Khazanov, G. V., and M. W. Liemohn, Non-steady-state ionosphere-plasmasphere coupling of superthermal electrons, *J. Geophys. Res., 100*, 9669, 1995.

Khazanov, G. V., M. A. Koen, Y. V. Konikov, and I. M. Sidorov, Simulation of ionosphere-plasmasphere coupling taking into account ion inertia and temperature anisotropy, *Planet. Space Sci., 32*, 585, 1984.

Khazanov, G. V., M. W. Liemohn, T. I. Gombosi, and A. F. Nagy, Non-steady-state transport of superthermal electrons in the plasmasphere, *Geophys. Res. Lett., 20*, 2821, 1993.

Khazanov, G. V., M. W. Liemohn, and T. E. Moore, Photoelectron effects on the self-consistent potential in the collisionless polar wind, *J. Geophys. Res., 102*, 7509, 1997a.

Khazanov, G. V., E. N. Krivorutsky, T. E. Moore, M. W. Liemohn, and J. L. Horwitz, Lower hybrid oscillations in multicomponent space plasmas subjected to ion cyclotron waves, *J. Geophys. Res.*, 102, 175, 1997b.

Khazanov, G. V., M. W. Liemohn, E. N. Krivorutsky, and T. E. Moore, Generalized kinetic description of a plasma in an arbitrary field-aligned potential energy structure, *J. Geophys. Res., 103*, 6871, 1998.

Kozyra, J. U., M.-C. Fok, E. R. Sanchez, D. S. Evans, D. C. Hamilton, and A. F. Nagy, The role of precipitation losses in producing the rapid early recovery phase of the Great Magnetic Storm of February 1986, *J. Geophys. Res., 103*, 6801, 1998.

Lawrence, D. J., M. F. Thomsen, J. E. Borovsky, and D. J. McComas, Measurements of early and late-time plasmasphere refilling as observed from geosynchronous orbit, *J. Geophys. Res.*, in press, 1999.

Liemohn, M. W., and G. V. Khazanov, Collisionless plasma modeling in an arbitrary potential energy distribution, *Phys. Plasmas, 5*, 580, 1998.

Liemohn, M. W., G. V. Khazanov, T. E. Moore, and S. M. Guiter, Self-consistent superthermal electron effects on plasmaspheric refilling, *J. Geophys. Res., 102*, 7523, 1997.

McIlwain, C. E., Plasma convection in the vicinity of the geosynchronous orbit, in *Earth's Magnetospheric Processes*, edited by B. M. McCormac, p. 268, D. Reidel, Hingham, Mass., 1972.

Miller, R. H., C. E. Rasmussen, T. I. Gombosi, G. V. Khazanov, and D. Winske, Kinetic simulation of plasma flows in the inner magnetosphere, *J. Geophys. Res., 98*, 19,301, 1993.

Ober, D. M., J. L. Horwitz, and D. L. Gallagher, Formation of density troughs embedded in the outer plasmasphere by subauroral ion drift events, *J. Geophys. Res., 102*, 14,595, 1997.

Olsen, R. C., S. D. Shawhan, D. L. Gallagher, J. L. Green, C. R. Chappell, and R. R. Anderson, Plasma observations at the Earth's magnetic equator, *J. Geophys. Res., 92*, 2385, 1987.

Olsen, R. C., L. J. Scott, and S. A. Boardsen, Comparison between Liouville's theorem and observed latitudinal distributions of trapped ions in the plasmapause region, *J. Geophys. Res., 99*, 2191, 1994.

Park, C. G., Whistler observations of the interchange of ionization between the ionosphere and protonosphere, *J. Geophys. Res., 75*, 4249, 1970.

Pierrard, V., and J. Lemaire, Lorentzian ion exosphere model, *J. Geophys. Res., 101*, 7923, 1996.

Rasmussen, C. E., and R. W. Schunk, Multistream hydrodynamic modeling of interhemispheric plasma flow, *J. Geophys. Res., 93*, 14,557, 1988.

Rasmussen, C. E., S. M. Guiter, and S. G. Thomas, A two-dimensional model of the plasmasphere: Refilling time constants, *Planet. Space Sci., 41*, 35, 1993.

Reynolds, M. A., G. Ganguli, J. A. Fedder, and D. J. Meléndez-Alvira, Effect of diurnal convection on trapped thermal plasma in the outer plasmasphere, *Geophys. Res. Lett. 24*, 2255, 1997.

Schulz, M., and M. C. Koons, Thermalization of colliding ion streams beyond the plasmapause, *J. Geophys. Res., 77*, 248, 1972.

Singh, N., Refilling of a plasmaspheric flux tube - Microscopic plasma processes, in *Modeling Magnetospheric Plasma, Geophys. Monogr. Ser.*, vol. 44, edited by T. E. Moore and J. H. Waite Jr., p. 87, AGU, Washington, D. C., 1988.

Singh, N., Role of ion temperature anisotropy in multistage refilling of the outer plasmasphere, *Geophys. Res. Lett., 18*, 817, 1991.

Singh, N., Effects of electrostatic ion cyclotron wave instability on plasma flow during early stage plasmaspheric refilling, *J. Geophys. Res., 101*, 17,217, 1996.

Singh, N., High altitude trapping of beam ions by self-generated plasma waves in interhemispheric plasma flows, *Geophys. Res. Lett., 25*, 1829, 1998.

Singh, N., and J. L. Horwitz, Plasmaspheric refilling: Recent observations and modeling, *J. Geophys. Res., 97*, 1047, 1992.

Singh, N., R. W. Schunk, and H. Thiemann, Temporal features of the refilling of a plasmaspheric flux tube, *J. Geophys. Res., 91*, 13,433, 1986.

Singh, N., G. R. Wilson, and J. L. Horwitz, Comparison of hydrodynamic and semikinetic treatments for a plasma flow along closed field lines, *J. Geophys. Res., 99*, 11,495, 1994.

Sojka, J. J., and G. I. Wrenn, Refilling of geosynchronous flux tubes as observed at the equator by GEOS 2, *J. Geophys. Res., 90*, 6379, 1985.

Sojka, J., R. W. Schunk, J. F. Johnson, J. H. Waite, and C. R. Chappell, Characteristics of thermal and superthermal ions associated with the dayside plasma trough as measured by the Dynamics Explorer retarding ion mass spectrometer, *J. Geophys. Res., 88*, 7895, 1983.

Song, X.-T., R. Gendrin, and G. Caudal, Refilling process in the plasmasphere and its relation to magnetic activity, *J. Atmos. Terr. Phys., 50*, 185, 1988.

Thomsen, M. F., J. E. Borovsky, D. J. McComas, and M. R. Collier, Variability of the ring current source population, *Geophys. Res. Lett., 25*, 3481, 1998.

Weiss, L. A., R. L. Lambour, R. C. Elphic, and M. F. Thomsen, Study of plasmaspheric evolution using geosynchronous observations and global modeling, *Geophys. Res. Lett., 24*, 599, 1997.

Wilson, G. R., J. L. Horwitz, and J. Lin, A semikinetic model for early stage plasmasphere refilling, 1: Effects of Coulomb collisions, *J. Geophys. Res., 97*, 1109, 1992.

Wrenn, G. L., J. J. Sojka, and J. F. E. Johnson, Thermal protons in the morning magnetosphere: Filling and heating near the equatorial plasmapause, *Planet. Space Sci., 32*, 351, 1984.

P. D. Craven, Space Sciences Laboratory, NASA/MSFC, Mail Code ES-83, Huntsville, AL 35812. (paul.craven@msfc.nasa.gov)

G. V. Khazanov, Geophysical Institute, University of Alaska Fairbanks, P.O. Box 757320, Fairbanks, AK 99775-7320. (khazanov@gi.alaska.edu)

J. U. Kozyra and M. W. Liemohn, Space Physics Research Laboratory, University of Michigan, 2455 Hayward Street, Ann Arbor, MI 48109-2143. (liemohn@umich.edu, jukozyra@umich.edu)

(Received December 9, 1998; revised February 15, 1999; accepted February 16, 1999.)